Check for updates

Isotopic components and source analysis of inorganic nitrogen in coastal aerosols of the Yellow Sea

Ke Zhang[1,2], Sumei Liu[1,2]*, Nian Wu[1,2] and Wenqi Xu[1]

[1]Key Laboratory of Marine Chemistry Theory and Technology Ministry of Education (MOE), Ocean University of China/Qingdao Collaborative Innovation Center of Marine Science and Technology, Qingdao, China, [2]Laboratory of Marine Ecology and Environmental Science, Qingdao National Laboratory for Marine Science and Technology, Qingdao, China

The coastal atmospheric environment is one of the most complex environments on earth. It is shaped by terrestrial, marine, and atmospheric processes and acts as an external nutrient source for coastal waters. At present, there are few observations of inorganic nitrogen isotopes of China coastal aerosols, let alone the Yellow Sea. In this study, a weekly collection of total suspended particulate aerosols was conducted on the Qianliyan Island in 2018 for the measurements of inorganic nitrogen species (NO_3^- and NH_4^+) and their isotopic ratios ($\delta^{15}N\text{-}NO_3^-$, $\delta^{18}O\text{-}NO_3^-$, and $\delta^{15}N\text{-}NH_4^+$). At the Qianliyan Island, the average NO_3^- and NH_4^+ concentrations were 2.49 $\pm$ 2.12 and 3.33 $\pm$ 2.68 $\mu g \cdot m^{-3}$, respectively; the average $\delta^{15}N\text{-}NO_3^-$, $\delta^{18}O\text{-}NO_3^-$, and $\delta^{15}N\text{-}NH_4^+$ were 2.4‰ $\pm$ 5.7‰, 78.7‰ $\pm$ 8.0‰, and −2.6‰ $\pm$ 6.3‰, respectively. The major nitrate formation pathways were •OH oxidation and N_2O_5 hydrolysis paths, and the dominant sources of inorganic nitrogen aerosols were coal combustion (29% $\pm$ 7%), marine (19% $\pm$ 15%), and fertilizer (16% $\pm$ 13%). Aerosol $\delta^{15}N\text{-}NO_3^-$ and $\delta^{18}O\text{-}NO_3^-$ were obviously higher in winter and lower in summer; conversely, aerosol $\delta^{15}N\text{-}NH_4^+$ was slightly higher in summer and slightly lower in winter. The difference in nitrogen sources was considered to be the best explanation for the aerosol $\delta^{15}N\text{-}NO_3^-$ and $\delta^{15}N\text{-}NH_4^+$ differences between summer and winter, of which coal combustion contributed the most. The seasonal difference in nitrate formation paths was considered to be the best explanation for the difference of Qianliyan aerosol nitrate $\delta^{18}O\text{-}NO_3^-$ between summer and winter. Aerosol inorganic nitrogen deposition flux was estimated to be 3.4 nmol $N \cdot m^{-2} \cdot s^{-1}$, which induced less than 1% to marine primary production, and aerosol inorganic nitrogen deposition, compared with N_2 fixation, contributed some 80% of $\delta^{15}N\text{-}NO_3^-$ depression of the summer Yellow Sea thermocline.

Introduction

Atmospheric nitrogen deposition is widely regarded as one of the important sources of nutrients in the marine system (Duce et al., 2008; Galloway et al., 2008). Aerosol has direct or indirect effects on climate, environment, and human health (Jickells et al., 2005; Pöschl, 2005; Das and Jayaraman, 2012; Xu and Penner, 2012; Seinfeld and Pandis, 2016). The rapid population growth has been egregiously negatively impacting on the coastal landscape and atmospheric environment in many parts of the world (Arteaga et al., 2019; Aswini and Hegde, 2021; Mohamed et al., 2021; Refulio-Coronado et al., 2021; Wang et al., 2021). For example, human activities have caused a large number of nutrients to be transported to the coastal waters, resulting in a surge in the concentration of inorganic nitrogen compared with that of phosphorus and the disharmony of nitrogen, phosphorus, and silicon in the coastal waters of China (Zhang et al., 2007b; Galloway, 2013; Qi et al., 2020). The weak exchange capacity of seawater on the continental shelf of China exacerbates the eutrophication of nearshore waters of China, resulting in the frequent occurrence of harmful algal blooms (Xin et al., 2019; Wang et al., 2021).

Anthropogenic/terrestrial dissolved inorganic nitrogen (DIN) sources commonly contain industrial and civil sources (coal combustion), agricultural sources (fertilizer, animal waste, and biomass burning), and transportation sources (road dust/soil and vehicle emission). As the distance increases from the shoreline, the nutrient concentrations in atmospheric total suspended particulate (TSP) aerosols decrease exponentially (Morin et al., 2009; Seok et al., 2021) and the anthropogenic/terrestrial contributions to seawater decrease. Therefore, the influence of anthropogenic/terrestrial DIN in aerosol on marginal sea is much greater than that on open sea. In addition to anthropogenic/terrestrial sources, the significance of a seawater-derived (named "marine-sourced") DIN, which is related to biological activities and acted on the atmosphere through the sea–air interface, has recently been recognized (Altieri et al., 2021; Dobashi et al., 2022). Surface seawater is considered to be the source of gaseous organic nitrogen and ammonia in the marine atmosphere (Altieri et al., 2013; Bertram et al., 2018; Altieri et al., 2021; Yu and Li, 2021). The marine emission of organic alkyl nitrates is converted into atmospheric NO_x and eventually nitrate (Burger et al., 2022). As marine atmospheric environment is acidic, ammonium is formed right after ammonia is discharged (Altieri et al., 2014). Therefore, it is necessary to consider both anthropogenic/terrestrial and marine sources for DIN in marginal-sea aerosols.

As the main species of aerosol DIN, nitrate and ammonium concentrations only provide information on DIN composition and deposition flux. The isotopic compositions of atmospheric inorganic nitrogen species are imperative to acquire further information, which goes far beyond the judgment based on the continental inorganic nitrogen species concentrations being

usually higher than those from marine. From the limited studies, the average $\delta^{15}N\text{-}NO_3^-$ values are more positive in the Pacific Ocean than that in the Atlantic Ocean, and the average aerosol $\delta^{18}O\text{-}NO_3^-$ values (70‰–85‰) are similar in the Atlantic Ocean and the Pacific Ocean (Morin et al., 2009; Kundu et al., 2010; Kawashima and Kurahashi, 2011; Gobel et al., 2013; Savarino et al., 2013; Kamezaki et al., 2019; Carter et al., 2021; Joyce et al., 2022), though the regularity is not shown for aerosol nitrate concentrations in the Atlantic Ocean when comparing with that in the Pacific Ocean, because sometimes nitrate concentration in the coastal area of Japan (Kawashima and Kurahashi, 2011) is even lower than that in the open Atlantic Ocean (28°S–52°N) (Morin et al., 2009). From even limited studies, it concludes that both aerosol ammonium concentrations and $\delta^{15}N\text{-}NH_4^+$ values were relatively higher in the Pacific Ocean than that in the Atlantic Ocean, whether in the coastal or open-sea atmosphere (Kundu et al., 2010; Kawashima and Kurahashi, 2011; Lin et al., 2016; Kamezaki et al., 2019; Joyce et al., 2022). In the open Atlantic Ocean (40°S–50°N), aerosol $\delta^{15}N\text{-}NH_4^+$ can be as low as −12‰ (Lin et al., 2016); in the marginal sea of the Western Pacific Ocean, aerosol $\delta^{15}N\text{-}NH_4^+$ can reach 38‰ (Kawashima and Kurahashi, 2011).

Along the marginal seas of China, the nitrate aerosol concentration decreases from the Bohai Sea to the South China Sea, with the aerosol nitrate concentrations of 6.0 ± 3.4 and 6.6 ± 2.7 µg·m^{-3}, respectively, in the Bohai Sea, and the boundary between the Bohai Sea and the Yellow Sea were (Zong et al., 2017; Zong et al., 2022) and as low as 0.5 ± 0.2 µg·m^{-3} in the South China Sea (Xiao et al., 2015). The variation of aerosol $\delta^{15}N\text{-}NO_3^-$ is opposite to that of $\delta^{18}O\text{-}NO_3^-$. From the Bohai Sea, the boundary between the Bohai Sea and the Yellow Sea to the South China Sea, annual average $\delta^{15}N\text{-}NO_3^-$ values were 7.8‰ ± 5.0‰, 8.3‰ ± 6.2‰, and 1.5‰ ± 1.6‰, respectively, and annual average $\delta^{18}O\text{-}NO_3^-$ values were 72.6‰ ± 13.5‰, 76.9‰ ± 11.8‰, and 83.2‰ ± 10.6‰, respectively. So far, there is no report on aerosol nitrogen isotope of ammonium over the Chinese marginal seas.

On these basis of DIN isotopic values and the developed methods, studies on stable nitrogen and oxygen isotopes have been used for source tracing and formation pathways (Walters and Michalski, 2015; Walters and Michalski, 2016; Elliott et al., 2019; Walters et al., 2019). In order to control coastal air pollution from the source, researches in coastal areas of China focused on source tracing. Coal combustion was the main source of aerosol nitrate in the South China Sea in cold months (October to January), whereas biomass burning, animal manure, and soil emission were the main sources of aerosol nitrate in the South China Sea in warm months (May to August) by comparison with the source values (Xiao et al., 2015). Coal combustion was also the main source of annual aerosol nitrate at the junction of the Yellow Sea and the Bohai Sea (36% ± 7%; Zong et al., 2017) and in the Bohai Sea (46% ± 16%; Zong et al., 2022). The less important contributors to aerosol nitrate were

biomass burning, vehicle emission, and soil emission. As coal-fire combustion has higher δ^{15}N-NO$_x$ relative to biomass burning and fertilized soil emission (Elliott et al., 2019), the annual low proportion of coal combustion contribution may be one of the reasons for the lower aerosol δ^{18}O-NO$_3^-$ in the South China Sea when compared with the Yellow Sea and the Bohai Sea. However, these studies exclude marine source in the source analysis, though marine source has its significance as previously mentioned. Tianjin, a coastal city east to the Bohai Sea, has an estimated marine source of ~4% in PM$_{2.5}$ (Dong et al., 2022). Usually, the contribution of marine source to TSP aerosols increases with the increase of aerosol particle size (Yeatman et al., 2001), making it reasonable to consider marine source for Qianliyan TSP aerosols. As for formation pathways of nitrate, estimation has been done that •OH oxidation and N$_2$O$_5$ hydrolysis paths contribute 41%–42% and 28%–41%, respectively, of total aerosol nitrate at a global scale (Alexander et al., 2020). Nitrate production in the winter equatorial Pacific atmosphere was dominated by •OH oxidation, and the portion ranged from 58% to 63% (Carter et al., 2021), which is comparable to the portion of •OH path for aerosol nitrate in summer Bohai Sea (Zong et al., 2022). However, the portion of •OH path for aerosol nitrate declined by 27% in the winter Bohai Sea (Zong et al., 2022). Therefore, it is necessary to discern the seasonal variation of nitrate formation path of Qianliyan.

In the view that dry deposition fluxes of inorganic nitrogen in atmospheric aerosols were well reported (Qi et al., 2020) but limited studies have reported the isotopic composition of nitrate and/or ammonium in coastal aerosols over the Chinese marginal seas, we report the aerosol nitrate and ammonium isotopes in the Yellow Sea. In order to avoid the degradation of coastal environment caused by excessive inorganic nitrogen deposition, we trace the sources of inorganic nitrogen in the Yellow Sea aerosol in consideration of marine source. In addition, we estimate the contribution of aerosol DIN deposition to marine primary production and the constrain of aerosol DIN isotopes on new nitrogen inputs to thermocline.

Materials and methods

Aerosol sampling

Aerosols are a mixing of terrigenous/anthropogenic and marine sources at the Qianliyan Island along the Yellow Sea coast of China, including the continental aerosols from China, Korea, and Japan, and marine aerosols from the North-West Pacific Ocean on the downwind of East Asian mass transport path controlled by the East Asian Summer and Winter Monsoon (Chang et al., 2021).

Aerosol samples were weekly collected (24 h per each time) by a high-volume sampler (Laoying 2031 typed intelligent large flow TSP sampler, Qingdao Laoying Environmental Technology

Co., Ltd) at a flow rate of 1.05 m^{-3}·min^{-1} with Whatman 41 filter at Qianliyan Island (36.27°N, 121.38°E) of the western Yellow Sea throughout 2018 and were subsequently frozen (−20°C) until they were determined. Aerosol sampling did carefully avoid precipitations because of the aerosol removal by precipitations (Yeatman et al., 2001).

Before and after sampling, the filters were weighed on electronic balance with the readability up to 0.01 mg (Sartorius CPA224S analytical lab balance, Sartorius, Göttingen, Germany) immediately after being in a desiccator (25°C, 10% relative humidity [RH]) to a constant weight. Constant weight refers to the weight difference of the filter dried twice in succession being less than 0.01 mg for a blank filter and 0.2 mg for a sampled filter. The second and subsequent weighing were carried out after further drying for 1 h under same conditions. Generally, drying for more than 24 h ensures constant filter weight.

Ultrasound extraction

Sampled filters were divided into 16 equal parts. One central fixed position portion of each sample was ultrasonically extracted for 1 h using Milli-Q water (18.2 MΩ·cm), and extractions were filtered by a disposable filter (0.45 µm).

Analytical method and quality control

Inorganic nitrogen concentrations

NO$_3^-$, NO$_2^-$and NH$_4^+$ concentrations were measured by the nutrient autoanalyzer (QuAAtro39-SFA, SEAL Analytical Group) with detection limits of 0.02, 0.01, and 0.02 µmol·L^{-1}, respectively, and all precisions (RSD) were less than 2%. Among all samples, NO$_2^-$ accounted for 0–0.1% of the sum of NO$_3^-$ and NO$_2^-$, with an average of 0.03% ± 0.03%. Hence, the results of NO$_2^-$ were not reported and were not deducted in raw results of NO$_3^-$ channel in this study. Since the proportions of NO$_2^-$ in the sum of NO$_3^-$ and NO$_2^-$ were less than 1%, NO$_2^-$ influence can be ignored when determining NO$_3^-$ isotopes (Casciotti and McIlvin, 2007).

Inorganic nitrogen isotopes

Additionally, nitrogen isotopic composition of nitrate was measured by the biochemical method based on the conversion of NO$_3^-$ to N$_2$O by denitrifying bacteria (*Pseudomonas aureofaciens*, ATC: 13958) (Sigman et al., 2001), and nitrogen isotopic composition of ammonium was measured by the chemical method based on the conversion of NH$_4^+$ to NO$_2^-$ and then to N$_2$O, which was then analyzed by isotope ratio mass spectrometry (IsoPrime 100, Elementar Analysensysteme GmbH) (Zhang et al., 2007a). The isotope ratios were calibrated against standard reference materials IAEA-N3

(δ^{15}N: +4.7‰, δ^{18}O: +25.6‰), USGS-34 (δ^{15}N: −1.8‰, δ^{18}O: −27.9‰), and USGS-35 (δ^{15}N: −1.8‰, δ^{18}O: +57.5‰) (Böhlke et al., 2003) and laboratory mixed standard spike (δ^{15}N: +14.3‰, δ^{18}O: −23.0‰) for nitrate nitrogen and oxygen isotopes and standard reference materials IAEA-N1 (δ^{15}N: +0.4‰), USGS-25 (δ^{15}N: −30.4‰), and USGS-26 (δ^{15}N: +53.7‰) for ammonium nitrogen isotopes (Böhlke et al., 1993). Correction to nitrate δ^{15}N for δ^{17}O contribution needed to be made because of the joint contribution of $^{14}N^{14}N^{17}O$ and $^{14}N^{15}N^{16}O$ to the peak at mass 45. The correction followed the steps of Hastings et al. (2003) and a better adjustment of δ^{17}O calculation by $\delta^{17}O = 0.86 \times \delta^{18}O + 0.05$ (Michalski et al., 2004). The standard solutions and blank samples were measured every 10 samples to make quality control. The deep water from the Mariana Trench (8,000 m in depth, δ^{15}N-NO$_3^-$: 5.2‰ ± 0.1‰, δ^{18}O-NO$_3^-$: 1.9‰ ± 0.2‰) and IAEA-N1 (δ^{15}N-NH$_4^+$: 0.43‰ ± 0.22‰) were measured in batches to assure the data quality. Based on replicate analyses of the standards and the unknowns, the average precisions of nitrogen and oxygen isotope delta values are ±0.2‰ and ±0.5‰, respectively, or better.

Data processing

Back trajectories

The online HYSPLIT trajectory model (https://www.ready.noaa.gov/) is used for the air-mass back trajectory of 72 h—72 h is in consideration of the annual mean lifetime of nitrate and ammonium in the troposphere against dry deposition to the earth's surface (Asman et al., 1998; Alexander et al., 2020). This model determines the height of the mixed (boundary) layer from the meteorological data set. In order to better capture the source characteristics of air-mass, the mid-boundary layer height (one half of the mixed layer height) that reflects the characteristics of the average boundary layer flow field is selected as the starting height, and four start times, which are the start time of each sample (T), T + 6 h, T + 12 h, and T + 18 h, for each sample are set.

A three-endmember model for nitrate formation

A three-endmember model (Walters and Michalski, 2016) is induced to clarify the nitrate formation paths. The model includes three formation paths, namely, •OH oxidation (NO$_2$ +•OH → HNO$_3$), N$_2$O$_5$ hydrolysis (N$_2$O$_5$ + H$_2$O → 2HNO$_3$), and hydrocarbon paths (NO$_3$ + R [DMS/hydrocarbons] → HNO$_3$). NO$_x$ reacts with different oxidants to produce NO$_3^-$. During the day, •OH is the main oxidant because of the strong solar radiation (Lelieveld et al., 2004); during the night, O$_3$ oxidation dominates and reacts with NO$_2$ to produce N$_2$O$_5$/NO$_3$ (Walters and Michalski, 2015). Based on N and O isotopic mass-balance and the assumptions that

atmospheric isotopic equilibrium is achieved between NO and NO$_2$ during the daytime, and NO$_2$, NO$_3$ and N$_2$O$_5$ during the nighttime, aerosol nitrates formed by •OH oxidation, N$_2$O$_5$ hydrolysis and hydrocarbon paths yield distinctive δ^{15}N-δ^{18}O (Walters and Michalski, 2016). The calculation formula of three-endmember values of δ^{15}N-NO$_3^-$ and δ^{18}O-NO$_3^-$ is written in Text S1, and the method for calculating the portions of nitrate formation paths (the Bayesian mixing model simmr) is introduced in the next section.

Bayesian mixing model

The simmr, a Bayesian stable isotope mixing model implemented in R, is applicable to the generic situation where data include N measurements on J isotopes with K (K > J + 1) sources. Similarly, simmr can be applied to quantify the respective contributions of three nitrate formation path on data set of two isotopes from seasonal samples. Based on the results of potential sources/nitrate formation paths identification, the contribution of each endmember is described as

$$X_{ij} = \sum_{k=1}^{K} F_k \left(S_{jk} + c_{jk} \right) + \epsilon_{ij} \tag{1}$$

$$S_{jk} \sim N \left(\mu_{jk}, \omega_{jk}^2 \right) \tag{2}$$

$$c_{jk} \sim N \left(\lambda_{jk}, \tau_{jk}^2 \right) \tag{3}$$

$$\epsilon_{ij} \sim N \left(0, \sigma_j^2 \right) \tag{4}$$

where X_{ij} is the isotopic value j (1, 2, 3, ⋯, J) of the mixture i (1, 2, 3, ⋯, N), F_k is the source/path k proportion derived from simmr, S_{jk} is the source value k (1, 2, 3, ⋯, K) on isotope j, c_{jk} is the fractionation factor for isotope j on source/path k, and ϵ_{ij} is the residual error representing the additional unquantified variation among individual mixtures; S_{jk} is normally distributed with mean μ_{jk} and standard deviation ω_{jk} c_{jk} is normally distributed with mean λ_{jk} and standard deviation τ_{jk} and ϵ_{ij} is normally distributed with mean 0 and standard deviation σ_j. The detail of simmr refers to Parnell et al. (2010). Because of the homology of inorganic nitrogen species (Dong et al., 2022) and distinct source ranges of δ^{15}N-NH$_4^+$–δ^{15}N-NO$_3^-$ from field source sampling (Table S1), it provides a solution to source apportionment of inorganic nitrogen in aerosols. As reported, biomass burning, coal combustion, vehicle emission, and soil emission were main sources for terrigenous aerosol nitrate (Xiao et al., 2015; Zong et al., 2017) and fertilizer, animal waste, vehicle emission, and coal combustion for terrigenous aerosol ammonium (Pan et al., 2016; Pan et al., 2020). Furthermore, marine impact cannot be ignored for Qianliyan aerosols due to marine–atmosphere exchange (Savoie and Prospero, 1982; O'Dowd, 2002). The nitrogen isotope compositions of expected sources are presented in Table S1, and the nitrogen and oxygen isotope compositions of three nitrate formation paths are depicted in Figure S1.

Results

Air-mass source characteristic

The computed back trajectories (n = 45) were categorized into two clusters (continental and maritime) that mainly based on the origins of air-masses and trajectories pathways (Figure S2). The continental cluster (n = 39) consisted three subclusters, which were the eastern (northeast to southeast, n = 2), the southern (southeast to west, n = 1), and the northern (west to northeast, n = 36) continental origins. The northern continental subcluster included the most backward trajectories that originated from the Siberian plateau of Russia *via* Mongolia and inland of the North China. The eastern continental subcluster included the most backward trajectories that originated from developed countries Japan and South Korea. The sole southern continental subcluster carried near-ground pollution from south China, which is well known as one of economically developed regions in China. The maritime cluster (n = 6) comprised two subclusters, which were the open-sea (n = 2) and marginal sea (n = 4) origins. The open-sea cluster referred to back trajectories from remote Pacific Ocean, which barely went through human activity zone, whereas the marginal-sea cluster referred to back trajectories mostly from the Yellow Sea and the sole one from Sea of East/Japan. On average, the TSP concentration of the maritime cluster (81 ± 59 $\mu g \cdot m^{-3}$) was lower than the continental cluster (171 ± 53 $\mu g \cdot m^{-3}$). Specifically, TSP concentrations of the eastern continental, southern continental, northern continental, open-sea, and marginal-sea subclusters were 159 ± 35, 198, 171 ± 54, 47 ± 13, and 98 ± 68 $\mu g \cdot m^{-3}$, respectively. This delineated the decent trend of atmospheric TSP concentrations from land to ocean; therefore, three continental subclusters were integrated as one in the following results and discussions.

NO_3^- and NH_4^+ concentrations

The NO_3^- concentrations ranged from 0.45 to 13.19 $\mu g \cdot m^{-3}$, with a numerical average of 2.49 ± 2.12 $\mu g \cdot m^{-3}$, and the NH_4^+ concentrations ranged from 0.41 to 16.47 $\mu g \cdot m^{-3}$, with a numerical average of 3.33 ± 2.68 $\mu g \cdot m^{-3}$. In addition, NO_3^- concentration positively and significantly correlated with NH_4^+ concentration (Table S2), which was expressed as $c_{NO_3^-}$ = 0.7047 × $c_{NH_4^+}$ + 0.1421 (R^2 = 0.793). Classified by the air-mass sources, NO_3^- and NH_4^+ concentration ranges were respectively 0.45–13.19 and 0.69–16.47 $\mu g \cdot m^{-3}$ for the continental cluster, 0.56–0.57 and 0.41–0.83 $\mu g \cdot m^{-3}$ for the open-sea cluster, and 0.83–2.69 and 1.12–5.81 $\mu g \cdot m^{-3}$ for the marginal-sea cluster. Different-orientation NO_3^- and NH_4^+ concentrations were not significantly different (NO_3^-: Kruskal–Wallis test, H = 5.7, p > 0.05; NH_4^+: Kruskal–Wallis test, H = 5.1, p > 0.05). Classified by seasons, average NO_3^- and NH_4^+ concentrations were the lowest in summer, which is consistent with the lowest concentration of TSP in summer (Figure S3). Specifically, average NO_3^- concentration was 3.2 ± 3.1 $\mu g \cdot m^{-3}$ in spring, 1.3 ± 0.7 $\mu g \cdot m^{-3}$ in summer, 3.4 ± 1.7 $\mu g \cdot m^{-3}$ in autumn, and 1.9 ± 1.3 $\mu g \cdot m^{-3}$ in winter, whereas average NH_4^+ concentration was 4.4 ± 3.8 $\mu g \cdot m^{-3}$ in spring, 2.3 ± 1.8 $\mu g \cdot m^{-3}$ in summer, 3.9 ± 2.4 $\mu g \cdot m^{-3}$ in autumn, and 2.6 ± 1.4 $\mu g \cdot m^{-3}$ in winter at the Qianliyan Island (Figure S3). Seasonal NO_3^- concentrations were significantly different (Kruskal–Wallis test, H = 11.1, p < 0.05), whereas seasonal NH_4^+ concentrations were not significantly different (Kruskal–Wallis test, H = 5.3, p > 0.05).

$\delta^{15}N$ values of NO_3^- and NH_4^+

To sum up, $\delta^{15}N-NO_3^-$ in Qianliyan aerosols ranged from −5.5‰ to 14.1‰, with a numerical average of 2.4‰ ± 5.7‰, and $\delta^{15}N-NH_4^+$ ranged from −17.1‰ to 12.1‰, with a numerical average of −2.6‰ ± 6.3‰ (Figure 1). Classified by the air-mass sources, the arithmetic means of $\delta^{15}N-NO_3^-$ and $\delta^{15}N-NH_4^+$ were 1.8‰ ± 1.1 ‰ and −9.6‰ ± 2.6‰ for the open-sea cluster, −2.0‰ ± 2.5‰ and −3.6‰ ± 2.6‰ for the marginal-sea cluster, and 2.9‰ ± 5.8‰ and −2.2‰ ± 6.5‰ for the continental cluster at the Qianliyan Island (Figure 2). Different-orientation $\delta^{15}N-NO_3^-$ and $\delta^{15}N-NH_4^+$ values were not significantly different ($\delta^{15}N-NO_3^-$: Kruskal–Wallis test, H = 3.2, p > 0.05; $\delta^{15}N-NH_4^+$: Kruskal–Wallis test, H = 3.5, p > 0.05). Classified by seasons, the numerical average of $\delta^{15}N-NO_3^-$ was 1.3‰ ± 4.5‰ in spring, −2.2‰ ± 2.6‰ in summer, 0.3‰ ± 3.8‰ in autumn, and 9.2‰ ± 3.8‰ in winter, whereas the numerical average of $\delta^{15}N-NH_4^+$ was −0.6‰ ± 6.9‰ in spring, −0.8 ± 7.7‰ in summer, −4.2 ± 5.5 ‰ in autumn and was −5.1 ± 3.9‰ in winter at the Qianliyan Island (Figure S3). Seasonal $\delta^{15}N-NO_3^-$ values were significantly different (Kruskal–Wallis test, H = 24.0, p < 0.05), whereas seasonal $\delta^{15}N-NH_4^+$ values were not significantly different (Kruskal–Wallis test, H = 4.2, p > 0.05).

$\delta^{18}O$ values of NO_3^-

To sum up, $\delta^{18}O-NO_3^-$ in Qianliyan aerosols ranged from 63.3‰ to 98.0 ‰, with a numerical average of 78.7‰ ± 8.0‰ (Figure 1). Classified by the air-mass sources, the arithmetic mean of $\delta^{18}O-NO_3^-$ was 64.1‰ ± 1.1‰ for the open-sea cluster, 74.9‰ ± 3.7‰ for the marginal-sea cluster, and 81.4‰ ± 6.9‰ for the continental cluster at the Qianliyan Island (Figure 2). Different-orientation $\delta^{18}O-NO_3^-$ showed significant difference (Kruskal–Wallis test, H = 7.6, p < 0.05). Classified by seasons, the numerical average of $\delta^{18}O-NO_3^-$ was 78.6‰ ± 4.7‰ in spring, 70.5‰ ± 5.4 ‰ in summer, 80.3‰ ± 6.1 ‰ in autumn, and 84.4‰ ± 8.8 ‰ in winter at the Qianliyan Island (Figure S3). Seasonal $\delta^{18}O-NO_3^-$ showed significant difference (Kruskal–Wallis test, H = 17.6, p < 0.05).
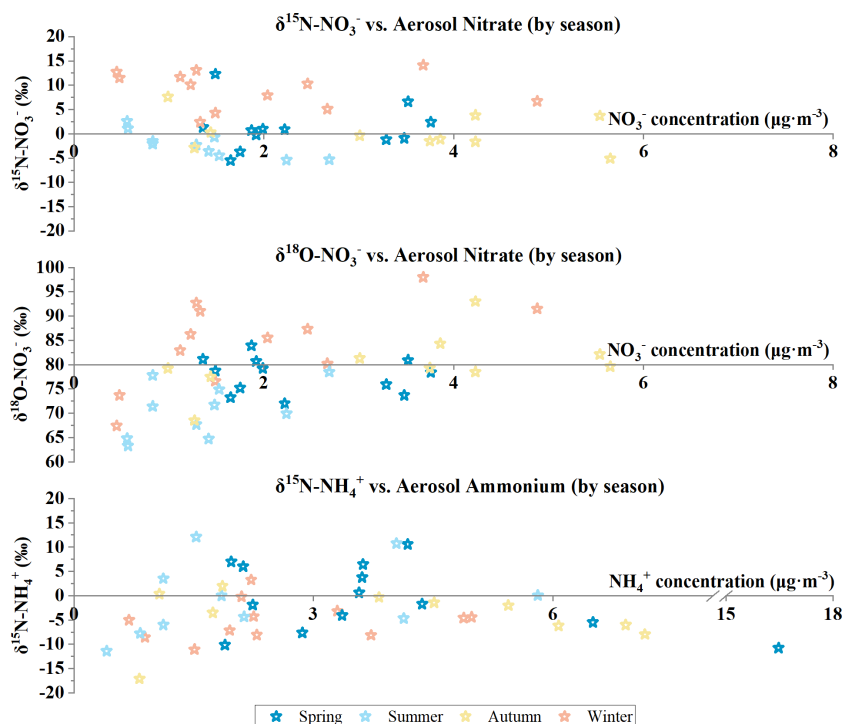
FIGURE 1
Aerosol nitrate and ammonium isotopic compositions plotted against aerosol nitrate and ammonium concentrations with samples coded by seasons at the Qianliyan Island in 2018.

Nitrate formation path

Inferred from a three-endmember model, the results showed that •OH oxidation and N_2O_5 hydrolysis paths were two main formation pathways for aerosol nitrate formation (Figure 3). The average contribution of the •OH oxidation path was high in summer (74.9 ± 4.7%) and low in winter (41.2 ± 7.0%); N_2O_5 hydrolysis path was low in summer (12.6 ± 5.9%) and high in winter (53.8 ± 7.6%), indicating a transition of the leading pathway of nitrate formation from the •OH oxidation in summer to the O_3 oxidation in winter because N_2O_5 was produced by O_3, which reacts with NO_2.

Inorganic nitrogen source apportionment

Annually, the dominant sources of inorganic nitrogen were coal combustion (29% ± 7%), marine (19% ± 15%), and fertilizer (16% ± 13%) (Figure 4). The highest proportion of coal burning in winter, the highest portion of marine source in summer, and the lowest proportion of fertilizer in winter were the three main characteristics of the seasonal sources of inorganic nitrogen isotopes. The primary source of Qianliyan inorganic nitrogen

aerosols was coal combustion in winter (55% ± 6%), which acted in concert with the heating period. On the contrary, fertilizer accounted for the smallest proportion in winter (9% ± 8%), which acted in concert with the agricultural activity inactive period. Marine contribution was slightly raised to 25% ± 20% in summer but diminished to 10% ± 7% in winter, which is consistent with the dominant wind direction controlled by the East Asian monsoon.

Discussions

Interpretations for seasonal variations of aerosol inorganic nitrogen isotopes

Seasonal $\delta^{15}N\text{-}NO_3^-$ variation

The seasonal characteristic of Qianliyan aerosol nitrate $\delta^{15}N\text{-}NO_3^-$ is that its value was significantly higher in winter and lower in summer, which was common in aerosols over Northwest Pacific marginal seas near Qianliyan (Figure 5) and the other seas (Savarino et al., 2013; Li et al., 2021). Additionally, it was also observed that the patterns of $\delta^{15}N\text{-}NO_3^-$ and $\delta^{18}O\text{-}NO_3^-$ are higher in winter and lower in summer in aerosols over land (Zhao et al., 2020; Zhu et al., 2021; Dong et al., 2022;
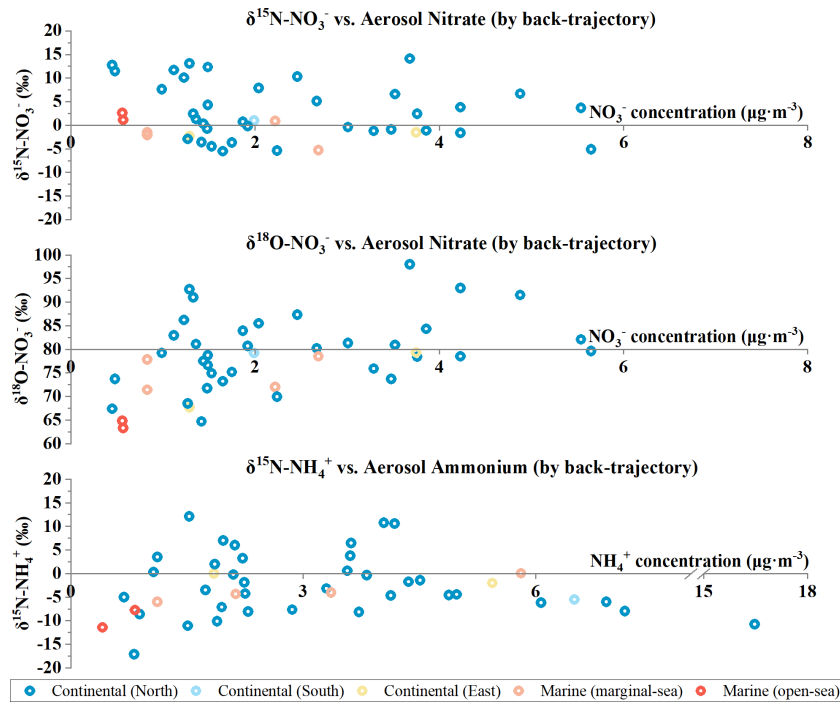
FIGURE 2

Aerosol nitrate and ammonium isotopic compositions plotted against aerosol nitrate and ammonium concentrations with samples coded based on the air-mass back trajectories at the Qianliyan Island in 2018.
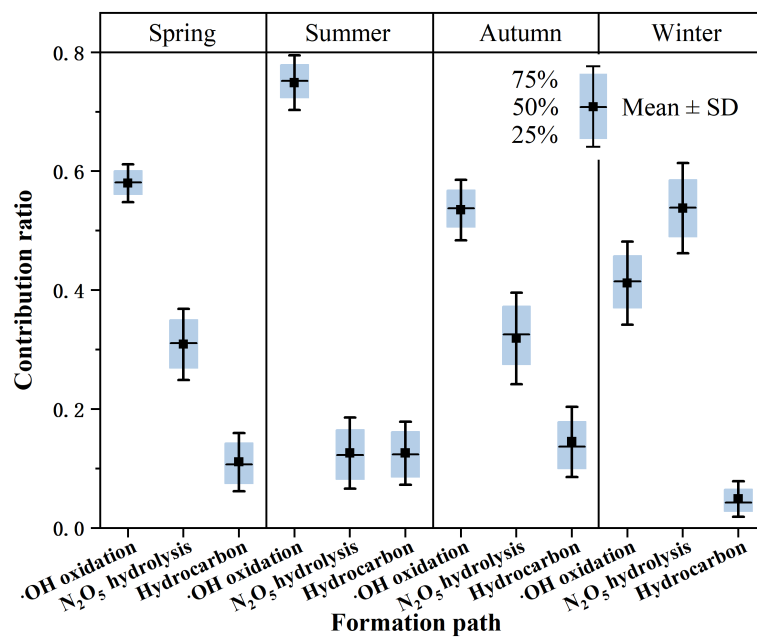
FIGURE 3

Contribution ratios of •OH oxidation, N_2O_5 hydrolysis and hydrocarbon paths for aerosol nitrate in different seasons at the Qianliyan Island.

FIGURE 4

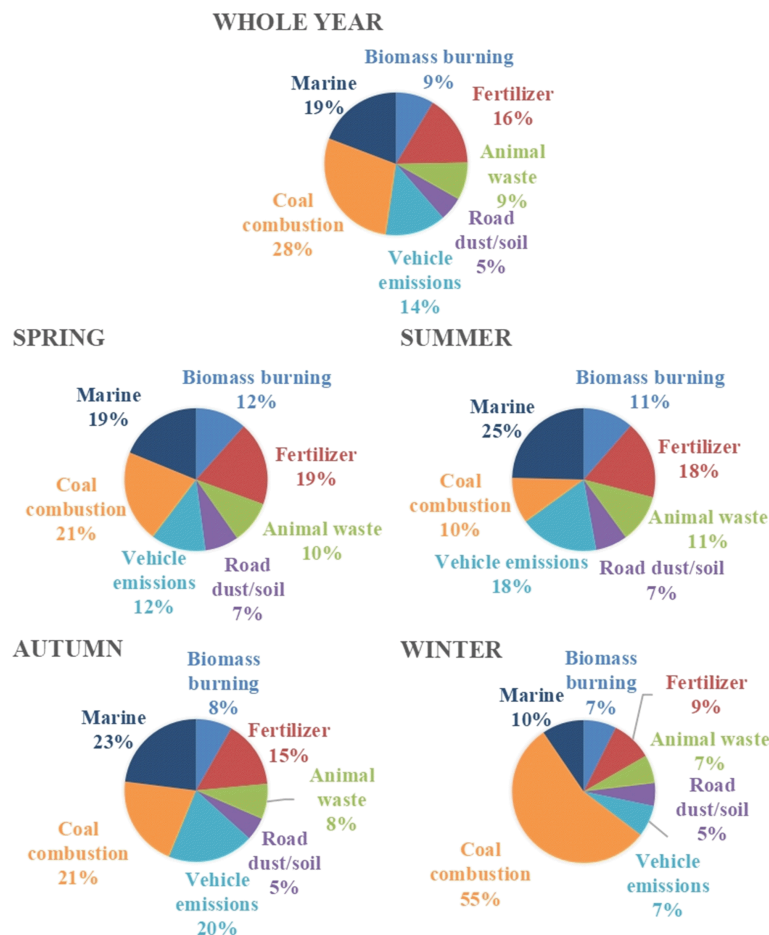Source apportion *via* bi-nitrogen isotopes of aerosol nitrate and ammonium at the Qianliyan Island.

Luo et al., 2022). For example, average $\delta^{15}N\text{-}NO_3^-$ values of aerosols in the Beijing–Tianjin–Hebei region with serious air pollution were 10.8‰ ± 3.6‰ in winter and −0.4‰ ± 2.8‰ in summer (Dong et al., 2022). These observational results indicate that there might exist unified reasons for the nitrate nitrogen isotope seasonality difference, regardless of the values of NO_3^- concentration and $\delta^{15}N\text{-}NO_3^-$ in different sites and the difference values of $\delta^{15}N\text{-}NO_3^-$ in summer and winter being different.

At the Qianliyan Island, the difference of average nitrate $\delta^{15}N\text{-}NO_3^-$ in aerosols between summer and winter was 11.4‰. Nitrate $\delta^{15}N\text{-}NO_3^-$ in Qianliyan aerosol exhibited negative correlations with temperature, RH, and sunshine hour (Table S2), showing a significant sensitivity to temperature, RH, and sunshine hour. Based on current cognition, aerosol nitrate $\delta^{15}N\text{-}NO_3^-$ are affected by source $\delta^{15}N\text{-}NO_x$ (Elliott et al., 2007; Elliott et al., 2019) and ^{15}N isotope fractionation during the conversion of NO_x oxidation to nitrate, of which ^{15}N isotope fractionation coefficients during nitrate transformation were related to

temperature and formation pathway (Freyer, 1991; Morin et al., 2009; Walters and Michalski, 2015; Walters and Michalski, 2016; Li et al., 2019 and references therein). Because both NO_x sources (e.g., fertilizer related to agricultural activities and coal combustion related to winter heating) and ^{15}N isotope fractionations during the conversion of NO_x oxidation to nitrate had seasonality, it needs further distinguishment of the effects of temperature, nitrate formation path, and NO_x source.

The nitrogen isotope fractionation of nitrate caused by the temperature difference of Qianliyan between summer and winter was 3.9‰ at large based on the isotope fractionation theory (Walters and Michalski, 2015), which is far less than the difference of average $\delta^{15}N\text{-}NO_3^-$ of Qianliyan aerosols between summer and winter. The nitrogen isotope fractionation of nitrate caused by the nitrate formation path variation of Qianliyan between summer and winter was 12.0‰ at large using the average portions of three nitrate formation paths that inferred from a three-endmember model with the fixed $\delta^{15}N\text{-}NO_x$ and temperature. However, it was reported that the
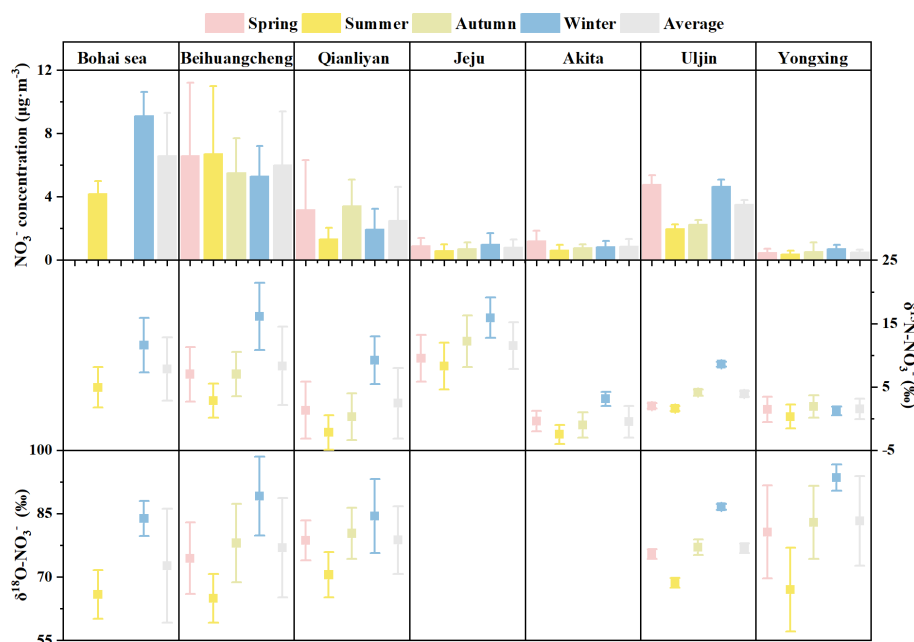
FIGURE 5

The seasonal and annual average ($\pm$ SD) of nitrate concentrations ($\mu g \cdot m^{-3}$) and nitrogen and oxygen isotopic compositions (‰) of nitrate over the marginal seas of China and the East/Japan sea. Data source: the Bohai Sea (Zong et al., 2022), Beihuangcheng (Zong et al., 2017), Jeju (Kundu et al., 2010), Akita (Kawashima, 2019), Uljin (Kim et al., 2019), and Yongxing (Xiao et al., 2015).

seasonality of $\delta^{15}N\text{-}NO_3^-$ was largely explained by source change rather than isotopic fractionation driven by NO_x photochemical equilibrium at Shenyang, a Chinese megacity (Li et al., 2019).

The $\delta^{15}N\text{-}NO_3^-$ difference caused by the NO_x sources of Qianliyan between summer and winter was 11.1‰ using the average source $\delta^{15}N\text{-}NO_3^-$ and the average portions of each source *via* simmr. Among all the sources, the proportions of coal and marine varied greatly in summer and winter. Compared with summer, the proportion of coal increased by 45%, and that of sea source decreased by 15% in winter, which multiplied with their source $\delta^{15}N\text{-}NO_3^-$ were 8.7‰ and 0.3‰, respectively. According to the Winter Clean Heating Plan in Northern China (2017–2021) (https://www.gov.cn/xinwen/2017-12/20/5248855/files/7ed7d7cda8984ae39a4e9620a4660c7f.pdf), the annual consumption of coal for heating during winter in the Northern China was approximately equivalent to 4×10^8 t of standard coal, and according to the China Energy Stastical Yearbook (2019) (www.stats.gov.cn/tjsj/ndsj/2019/indexch.htm), the national coal consumption was 27.38×10^8 t of standard coal in 2018. Thus, in winter, coal combustion was the primary source of the North China nitrate aerosols (59% $\pm$ 14%; Fan et al., 2020) and the primary source of the Bohai Sea nitrate aerosols (57% $\pm$ 11%; Zong et al., 2022). This meant that coal burning preferred to have the greatest impact on $\delta^{15}N\text{-}NO_3^-$ difference between summer and winter.

At other sites over the marginal seas of the Northwest Pacific, the minimum of the difference of average nitrate $\delta^{15}N\text{-}NO_3^-$ in aerosols between summer and winter was 0.9‰ at the South China Sea (Yongxing), and the maximum was 13.3 ‰ at the junction of the Yellow Sea and the Bohai Sea (Figure 5). The observed average temperature in East Asia was 18.9°C in summer and −7.5°C in winter (Jiang et al., 2005), which the temperature-dependent isotope fractionation seemed enough for small $\delta^{15}N\text{-}NO_3^-$ difference between winter and summer in the South China Sea aerosol though it was also necessary to exclude the impact of changes in sources and formation pathways. If the difference of average nitrate $\delta^{15}N\text{-}NO_3^-$ in aerosols between summer and winter exceeded 3.1‰, the changes in sources and formation pathways existed. However, in view of the information that we have at this moment, it is still difficult to identify the influences of the source and formation path.

Seasonal $\delta^{18}O\text{-}NO_3^-$ variation

The seasonal characteristic of Qianliyan aerosol nitrate $\delta^{18}O\text{-}NO_3^-$ is that its value was significantly higher in winter and lower in summer, which was common in aerosols over Northwest Pacific marginal seas near Qianliyan (Figure 5) and the other seas (Savarino et al., 2013; Li et al., 2021). Additionally, it was also observed that the patterns of $\delta^{18}O\text{-}NO_3^-$ are higher in winter and lower in summer in aerosols over land (Zhao et al., 2020; Zhu et al., 2021; Dong et al., 2022; Luo et al., 2022). For

example, average $\delta^{18}O$-NO_3^- of aerosols in an industrial base of Northeast China, Chang Chun, was 70.5‰ ± 10.0‰ in winter and 58.7‰ ± 4.5‰ in summer (Zhao et al., 2020). These observational results indicate that there might exist consistent reasons for the nitrate oxygen isotope seasonality difference, regardless of the values of NO_3^- concentration and $\delta^{18}O$-NO_3^- in different sites and the difference values of $\delta^{18}O$-NO_3^- in summer and winter being different.

At the Qianliyan Island, the difference of average nitrate $\delta^{18}O$-NO_3^- in aerosols between summer and winter was 13.9‰. Nitrate $\delta^{18}O$-NO_3^- in Qianliyan aerosol exhibited negative correlations with temperature, RH, and sunshine hour (Table S2), showing a significant sensitivity to temperature, RH, and sunshine hour. Based on current cognition, aerosol nitrate $\delta^{18}O$-NO_3^- are affected by source $\delta^{18}O$-NO_x, $\delta^{18}O$-H_2O, and ^{18}O isotope fractionation during the conversion of NO_x oxidation to nitrate, of which ^{18}O isotope fractionation coefficients during nitrate transformation were related to temperature and formation pathway (Walters and Michalski, 2016 and references therein). Because both NO_x sources, $\delta^{18}O$-H_2O and ^{18}O isotope fractionations during the conversion of NO_x oxidation to nitrate, had seasonality, it needs further distinguishment.

The oxygen isotope fractionation of nitrate caused by the temperature difference of Qianliyan between summer and winter was 2.5‰ at large based on the isotope fractionation theory (Walters and Michalski, 2016), which is far less than the difference of average $\delta^{18}O$-NO_3^- of Qianliyan aerosols between summer and winter. The oxygen isotope fractionation of nitrate caused by the nitrate formation path variation of Qianliyan between summer and winter was 17.1‰ at large using the average portions of three nitrate formation paths that inferred from a three-endmember model with the fixed $\delta^{18}O$-NO_x, $\delta^{18}O$-H_2O, and temperature. Generally, seasonal effect on $\delta^{18}O$-H_2O is that $\delta^{18}O$-H_2O is positively correlated with the temperature, which varies from about 0‰ per °C at the equator and about 0.5‰ per °C at the high latitudes (http://www-naweb.iaea.org/napc/ih/documents/global_cycle/vol%20II/cht_ii_04.pdf). At the Qianliyan Island, a midlatitude region, $\Delta\delta^{18}O$-H_2O predicts to be 0.25‰ per °C, and the calculated $\delta^{18}O$-NO_3^- difference that was caused by $\delta^{18}O$-H_2O between summer and winter was 2.9‰ at large, because at most one third of the oxygen atoms in nitrate come from the oxygen atoms in water. As for source $\delta^{18}O$-NO_x values, few studies have measured the nitrogen isotope of NO_x and the oxygen isotope at the same time (Felix and Elliott, 2014; Walters et al., 2018), because NO_x is emitted to the atmosphere primarily as NO, and it will be oxidized to NO_2 by oxidants, of which O_3 oxidation accounts for 84%–85% of global total oxidation paths and HO_2/RO_2 oxidation accounts for 14%–15% (Alexander et al., 2020). Reported $\delta^{18}O$-O_3 (95‰–130‰) is much larger than $\delta^{18}O$-RO_2 (~23‰) (Lee 2019 and references therein). Thus, the enrichment of the O-atoms in terminal positions of O_3 is

believed to be transferred to various NO_x species and to nitrate during oxidation by O_3, which means that the characteristics of source $\delta^{18}O$-NO_x will be replaced (Machalski et al., 2014). All in all, the formation path of nitrate has the greatest influence on aerosol $\delta^{18}O$-NO_3^- of Qianliyan.

At other sites over the marginal seas of the Northwest Pacific, the difference of average nitrate $\delta^{18}O$-NO_3^- in aerosols between summer and winter exceeded that of Qianliyan (Figure 5). The oxygen isotope fractionation of nitrate caused by the temperature difference of East Asia between summer and winter was 2.0‰ at large. Meanwhile, the influence of the $\delta^{18}O$-H_2O variation caused by temperature on $\delta^{18}O$-NO_3^- difference is 0–4.4 ‰. These two factors were too small to explain the $\delta^{18}O$-NO_3^- difference between summer and winter of 18.0‰–26.5‰ at fixed stations. Because source $\delta^{18}O$-NO_3^- will be eliminated by oxidants, it is believed that the formation path of nitrate has the greatest influence on aerosol $\delta^{18}O$-NO_3^-. The seasonal distribution of •OH concentration is higher in summer and lower in winter (Bahm and Khalil, 2004; Zong et al., 2017). On the contrary, O_3 concentration is high in summer and low in winter (Chen et al., 2022); The average contribution of the •OH pathway to nitrate aerosol in summer is expected to decrease in winter. For example, Zong et al. (2022) reported that the average contribution of the •OH pathway to nitrate aerosol was 61.8% ± 18.3% in summer and was 36.3% ± 20.6% in winter over the Bohai Sea. Zhao et al. (2020) reported that the estimated average contribution of the •OH pathway for fine nitrate aerosols in northeast China accounted for a relatively high proportion in all seasons, with the annual average contribution of 61.0% ± 18.8%, especially 79.4% ± 6.1% in summer. Xiao et al. (2020) reported that the estimated average contribution of •OH oxidation, N_2O_5 hydrolysis, and hydrocarbon paths for fine nitrate aerosols in autumn and early winter in southeast China were 37.1% ± 33.4%, 60.3% ± 32.2%, and 2.6% ± 2.7%, respectively. In winter, the equator has the longest sunshine duration relative to the Northern Hemisphere, thus aerosol nitrate production in the equatorial Pacific atmosphere is dominated by •OH oxidation (60%) in winter (Carter et al., 2021). However, Kamezaki et al. (2019) reported that the estimated average contribution of •OH oxidation, N_2O_5 hydrolysis, and hydrocarbon paths for fine nitrate aerosols over Pacific Ocean (40°S–65°N) were 76% ± 12%, 5% ± 6%, and 18% ± 7%, respectively, without obvious difference in summer and winter. They explained that •OH oxidation paths dominating in winter was because of the warm-period sampling. If the difference of average nitrate $\delta^{18}O$-NO_3^- in aerosols between summer and winter exceeded 4.4%, the formation path of nitrate accounts over source and temperature.

Seasonal $\delta^{15}N$-NH_4^+ variation

Unlike $\delta^{15}N$-NO_3^-, Qianliyan aerosol ammonium $\delta^{15}N$-NH_4^+ had no obvious significant correlation with meteorological

parameters (Table S2). Although the seasonal and different-orientation δ^{15}N-NH$_4^+$ of Qianliyan aerosols were not significantly different, average δ^{15}N-NH$_4^+$ of Qianliyan aerosols was slightly higher in summer and lower in winter like other coastal sites, Baengnyeong, Jeju, and Akita (Figure 6). Additionally, it was also observed that the patterns of δ^{15}N-NH$_4^+$ are higher in summer and lower in winter in aerosols over land (Park et al., 2018; Wu et al., 2019b; Dong et al., 2022). The average δ^{15}N-NH$_4^+$ difference in aerosols between summer and winter was low to 0.3‰ in Seoul, Korea (Park et al., 2018), and up to 36.6‰ in Tianjin, China (Dong et al., 2022). These observational results indicate that there might exist accordant reasons for the ammonium isotope seasonality difference, regardless of the values of NH$_4^+$ concentration and δ^{15}N-NH$_4^+$ in different sites and the differences of δ^{15}N-NH$_4^+$ in summer and winter being different.

Because N is conserved during the nonoxidation reaction of gaseous NH$_3$ to particulate NH$_4^+$ in the atmosphere, to a large extent, δ^{15}N-NH$_4^+$ reflects the sources of NH$_3$ (Elliott et al., 2019). For example, summer heavier δ^{15}N-NH$_4^+$ in Akita aerosol was explained by animal wastes (Kawashima and Kurahashi, 2011); summer heavier δ^{15}N-NH$_4^+$ in Jeju aerosols was partly explained by biomass burning with enriched ^{15}N from China-originated air-masses (Kundu et al., 2010). In addition, aerosol ammonium δ^{15}N-NH$_4^+$ is affected by ^{15}N isotope fractionation from NH$_3$ to NH$_4^+$. The negative kinetic isotope fraction (-28‰; Pan et al., 2016) occurs when gaseous NH$_3$ unidirectionally reacts with gaseous H$_2$SO$_4$, whereas the positive equilibrium isotope fraction occurs when gaseous NH$_3$ reversibly reacts with gaseous HCl or HNO$_3$ or H$_2$O under rich ammonia environment (NH$_3$/H$_2$SO$_4$ molar ratio > 2) between atmospheric NH$_4^+$ and gaseous NH$_3$ (Walters et al., 2019 and references therein). Since sufficient observations

showed that δ^{15}N values were sorted as δ^{15}N-NH$_4^+$ (solid, s), δ^{15}N-NH$_4^+$ (liquid, l), δ^{15}N-NH$_3$ (gas, g) from big to small (Savard et al., 2017; Ti et al., 2018; Zheng et al., 2018; Kawashima, 2019), the negative kinetic isotope effect on aerosol NH$_4^+$ must be washed out as equilibrium conditions are established between gaseous NH$_3$ and aerosol NH$_4^+$. The equilibrium fractionation factors can be theoretically estimated as $^{15}\epsilon_{NH_{4(aq)}^+/NH_{s(g)}} = 14058/T(K) - 12.20$ and $^{15}\epsilon_{NH_{4(s)}^+/NH_{s(g)}} = 12522/T(K) - 11.31$ (Walters et al., 2019), and theoretical calculations are confirmed as calculated values at 25°C($^{15}\epsilon_{NH_{4(aq)}^+/NH_{s(g)}}$: 35 ‰; $^{15}\epsilon_{NH_{4(s)}^+/NH_{s(g)}}$: 30 ‰) are largely identical to the chamber experiment result $^{15}\epsilon_{NH_{4(aerosol)}^+/NH_{s(g)}}$: 33 ‰, Heaton et al., 1997). The sources of NH$_3$ and ^{15}N isotope fractionation during the conversion of NH$_3$ oxidation to ammonium had seasonality, and both factors may lead to aerosol δ^{15}N-NH$_4^+$ difference between summer and winter.

At the Qianliyan Island, the difference of average ammonium δ^{15}N-NH$_4^+$ in Qianliyan aerosol between summer and winter was 4.3‰. Temperature and the NH$_3$ concentration level affect the chemical processes of NH$_3$ to NH$_4^+$. However, the correlations between ammonium δ^{15}N-NH$_4^+$ in Qianliyan aerosols and ambient temperature, RH, and sunshine hour were not significant (Table S2), which implied that the reason for the trend cannot be explained by temperature alone. For ^{15}N isotope fractionation from NH$_3$ to NH$_4^+$, the effect of RH can be negligible (Kawashima and Ono, 2019), and the influence of temperature was opposite to the seasonal trend of δ^{15}N-NH$_4^+$ of Qianliyan aerosols. Hence, it can be inferred that the seasonal variation of NH$_3$ sources had the greatest impact on the seasonal variation of ammonium δ^{15}N-NH$_4^+$ in Qianliyan aerosols.

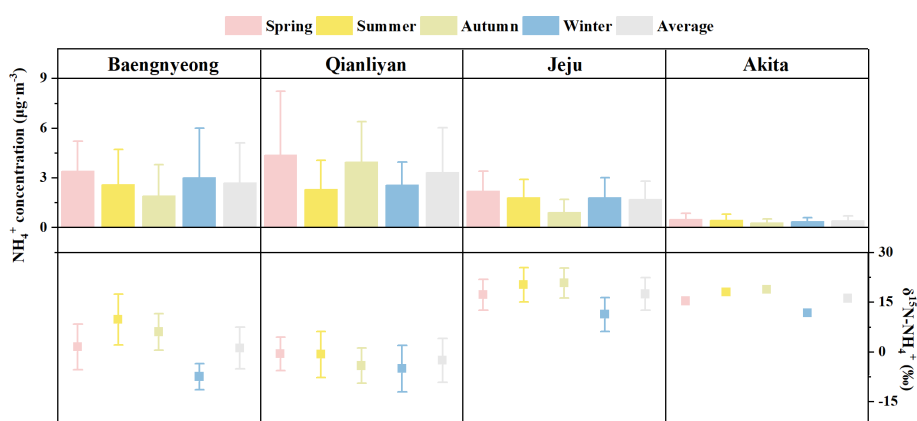The seasonal impress of δ^{15}N-NH$_3$ source had been recognized with a laboratory study pointing out that δ^{15}N-

FIGURE 6
The seasonal and annual average ($\pm$ SD) ammonium concentrations ($\mu g \cdot m^{-3}$) and nitrogen isotopic compositions (‰) of ammonium over the Yellow sea and the East/Japan sea. Data source: Baengnyeong (Park et al., 2018), Jeju (Kundu et al., 2010), and Akita (Kawashima, 2019).

NH$_3$ from agricultural activities might increase with the increase of temperature and ammonia loss (Schulz et al., 2001). However, it was difficult to be directly proved neither by NH$_3$ source apportion after the adjustment of field ^{15}N fractionation coefficients of the chemical transformation from gas NH$_3$ to aerosol NH$_4^+$ due to the lack of NH$_3$ concentrations and δ^{15}N-NH$_3$ values nor the emission and deposition list of NH$_3$ sources in this study. If ^{15}N isotope fractionation between gaseous NH$_3$ and aerosol NH$_4^+$ and the fraction of NH$_3$ that converted to NH$_4^+$ are known, the δ^{15}N-NH$_4^+$ for a certain source can be determined (Pan et al., 2016). Or observe the δ^{15}N-NH$_4^+$ for a certain source directly. At the Qianliyan Island, δ^{15}N-NH$_4^+$ of open-sea aerosols (−11.4‰ and −7.8‰) was apparently close to marine-source δ^{15}N-NH$_4^+$ (−10.2‰ to −2.2‰; David Felix et al., 2013). Thus, observed δ^{15}N-NH$_4^+$ values of various sources (Table S1) were used for source apportion in the absence of gas NH$_3$ concentrations and δ^{15}N-NH$_3$ values. The δ^{15}N-NH$_4^+$ difference caused by the sources of Qianliyan between summer and winter was 5.4‰ using the average source δ^{15}N-NH$_4^+$ and the average portions of each source via simmr. The largest seasonal source change of Qianliyan was reflected in the increased proportion of coal combustion in winter than that in summer. The enhanced fossil fuel source of ammonium aerosols of the South China (Wu et al., 2019b) and the dominant source of fossil fuel in winter ammonium aerosols in the North China (Pan et al., 2016) were found in the urban atmosphere. As one of the most abundant and affordable fossil fuels worldwide (64% in China in 2018, http://www.stats.gov.cn/tjsj/ndsj/2019/indexch.htm), it was reasonable to consider coal as the main source of ammonium in Qianliyan aerosols under the control of the East Asian winter monsoon. In addition, there were seasonal differences in fertilizer application because Chinese agricultural activities significantly decreased in winter due to the farming system, which was mainly dominated by one crop a year in the north (https://www.caas.cn/en/agriculture/agriculture_in_china/), and seasonal differences in marine contribution as the reversion of the dominant wind direction controlled by the East Asian monsoon. However, these two sources led to δ^{15}N-NH$_4^+$ difference of less than 1‰ using the average source δ^{15}N-NH$_4^+$ and the average portions of each source via simmr.

At other sites over the marginal seas of the Northwest Pacific, the difference of average ammonium δ^{15}N-NH$_4^+$ in aerosols between summer and winter exceeded that of Qianliyan (Figure 6), which the greater difference deduced the more pronounced seasonal change of NH$_3$/NH$_4^+$ sources. More research on seasonal source changes is needed to support this result. In addition, as a missing piece of all types of the isotope fraction, the transport isotope fraction of nitrogen species, which assumed it default to none in this study, has not been well studied so far and needs to be studied further.

Impacts of coastal aerosol inorganic nitrogen to the marginal sea

The concentration of nutrients in TSPs in the atmosphere decreased exponentially with the increase of the distance from the nearest land (Seok et al., 2021). Therefore, priority was give to the impact of coastal aerosol DIN on the Yellow Sea in this study.

Contribution to primary production

Aerosol DIN deposition flux is estimated by $F_{Dry}=C_{Dry}{\times}v_d$, of which C_{Dry} is the nutrient concentration and v_d is the nutrient deposition rate. The deposition rate of NO$_3^-$ and NH$_4^+$ are 1.15 and 0.6 cm·s^{-1}, respectively (Zhang et al., 2011 and references therein). At the Qianliyan Island, the deposition fluxes of aerosol nitrate and ammonium were 2.0 and 1.4 nmol N·m^{-2}·s^{-1}, respectively. The average dry deposition fluxes of nitrate and ammonium in atmospheric aerosols over the marginal seas and Northwest Pacific were 0.5 ± 0.3 and 0.7 ± 0.3 nmol N·m^{-2}·s^{-1}, respectively (Qi et al., 2020). Since the high fluxes of nitrate and ammonium were located in the Bohai Sea, the Yellow Sea, and the East China Sea, which were three to six times higher than those in the Northwest Pacific Ocean, our estimation of the deposition fluxes of nitrate and ammonium aerosol in the Yellow Sea were comparable to their results though a relatively low v_d for nitrate was used in the study of Qi et al. (2020).

The primary production was 0.3–0.8 mmol C·m^{-3}·h^{-1} on the Yellow Sea surface (Zhang et al., 2012). Also, the new primary production brought by aerosol DIN was overestimated to be 3.3 μmol C·m^{-3}·h^{-1} based on the Redfield ratio (C:N = 106:16). Thus, aerosol DIN deposition contributes less than 1% to primary production.

Impact on new nitrogen inputs to thermocline

The nutrient discharges from the atmosphere to the Yellow Sea were small compared with those from rivers, and aerosol DIN deposition flux was small compared with precipitation deposition flux (Liu et al., 2003). Since aerosol DIN dissolves quickly in seawater before deposits downward, aerosol DIN deposition rate was 0.7 μmol N·m^{-3}·h^{-1} above the thermocline (~20 m, Wu et al., 2019a), which was an order of magnitude higher than the reported average N$_2$ fixation rate of 72 nmol N·m^{-3}·h^{-1} on the Yellow Sea surface (Zhang et al., 2012).

The stratification of the Yellow Sea is obvious in summer, whereas the water mass is vertically uniform in winter. Based on summer observation on Yellow Sea, the mass weighted average δ^{15}N-NO$_3^-$ and δ^{15}N-NH$_4^+$ was −3.2‰ and 0.9‰, respectively. In total, the mass weighted average δ^{15}N-DIN was −0.7‰, which is lower to that by fixation N$_2$ (0.6‰; Yan et al., 2019) and is even lower than the average δ^{15}N-NO$_3^-$ of the Yellow Sea water

(7.0‰; Wu et al., 2019a). Thus, atmospheric low δ^{15}N-DIN may regulate ^{15}N on new nitrogen inputs to thermocline, resulting decreasing δ^{15}N-NO$_3^-$ under thermocline.

To quantitatively illustrate the relative contribution from atmospheric Nr and N$_2$ fixation to thermocline, we follow a similar approach adopted in Bermuda and Dongsha (Knapp et al., 2010; Yang et al., 2014) to estimate the fraction (f) of lowering nitrate δ^{15}N of the Yellow Sea thermocline induced by atmospheric DIN deposition. The f is written as f = $(\Delta\delta^{15}N_1 \times F_1)/$ $(\Delta\delta^{15}N_2 \times F_2 + \Delta\delta^{15}N_1 \times F_1))$, of which $\Delta\delta^{15}N_1$ is the difference of thermocline δ^{15}N-NO$_3^-$ (7‰) and aerosol δ^{15}N-DIN (−0.7‰), F$_1$ is aerosol DIN deposition flux (0.7 μmol N·m^{-3}·h^{-1}), $\Delta\delta^{15}N_2$ is the difference of thermocline δ^{15}N-NO$_3^-$ (7‰) and δ^{15}N newly fixed N$_2$ (−1‰, Karl et al., 1997), and F$_2$ is flux of fixed N$_2$ of thermocline (132 nmol N·m^{-3}·h^{-1}). This yields a value for f up to 83%, which is higher than those values at Bermuda and Dongsha (Knapp et al., 2010; Yang et al., 2014). Also, the influence of atmospheric active nitrogen deposition to lower δ^{15}N decreases with the increase of thermocline depth; the remainder of the ^{15}N depletion may result from the remineralization of N$_2$ fixation inputs. Note that a better perspective on the impact of the atmosphere on the nitrogen cycle in the Yellow Sea should consider atmospheric DON flux and its isotopic composition.

Conclusions

One-year collection of TSP aerosols was conducted on the Qianliyan Island in 2018 for the measurements of inorganic nitrogen species (NO$_3^-$ and NH$_4^+$) and their isotopic ratios (δ^{15}N-NO$_3^-$, δ^{18}O-NO$_3^-$ and δ^{15}N-NH$_4^+$). At the Qianliyan Island, the average NO$_3^-$ and NH$_4^+$ concentrations were 2.49 ± 2.12 and 3.33 ± 2.68 μg·m^{-3}; the average δ^{15}N-NO$_3^-$, δ^{18}O-NO$_3^-$ and δ^{15}N-NH$_4^+$ were 2.4‰ ± 5.7‰, 78.7‰ ± 8.0‰, and −2.6‰ ± 6.3‰, respectively.

Using the Bayesian mixing model, nitrate formation pathways and inorganic nitrogen source apportionment were obtained. At the Qianliyan Island, the major nitrate formation pathways in aerosols were •OH oxidation and N$_2$O$_5$ hydrolysis paths with a transition of the main pathway of nitrate formation from the •OH oxidation in summer to the O$_3$ oxidation in winter. Source apportion results make clear that terrigenous source and marine source accounted for about 80% and 20%, respectively, in Qianliyan inorganic nitrogen aerosols, of which the most dominant source was coal combustion (29% ± 7%). Additionally, three seasonal source characteristics of inorganic nitrogen isotopes were captured, which were the highest proportion of coal burning in winter, the highest portion of marine source in summer, and the lowest proportion of fertilizer in winter.

At the Qianliyan Island, aerosol δ^{15}N-NO$_3^-$ and δ^{18}O-NO$_3^-$ were obviously higher in winter and lower in summer;

on the contrary, aerosol δ^{15}N-NH$_4^+$ was slightly higher in summer and slightly lower in winter. Based on current cognition, aerosol nitrate δ^{15}N-NO$_3^-$ are coaffected by source δ^{15}N-NO$_x$ and ^{15}N isotope fractionation during the conversion of NO$_x$ oxidation to nitrate, including temperature and formation pathway. The seasonal difference in nitrogen sources was expected to be the best explanation for the difference of Qianliyan aerosol nitrate δ^{15}N-NO$_3^-$ between summer and winter, because the influence of temperature was too small and nitrogen was conservative during oxidation. Based on current cognition, aerosol nitrate δ^{18}O-NO$_3^-$ are coaffected by sources, including δ^{18}O-NO$_x$ and δ^{18}O-H$_2$O, and ^{15}N isotope fractionation during the conversion of NO$_x$ oxidation to nitrate, including temperature and formation pathway. The seasonal difference in nitrate formation paths was considered to be the best explanation for the difference of Qianliyan aerosol nitrate δ^{18}O-NO$_3^-$ between summer and winter, because the influence of temperature and δ^{18}O-H$_2$O was too small, and δ^{18}O-NO$_x$ was modified during oxidation. Based on current cognition, aerosol ammonium δ^{15}N-NH$_4^+$ is coaffected by source NH$_3$ and ^{15}N isotope fractionation during the conversion of NH$_3$ oxidation to ammonium. The seasonal difference in nitrogen sources was expected to be the best explanation for the difference of Qianliyan aerosol ammonium δ^{15}N-NH$_4^+$ between summer and winter, because the correlation of temperature and δ^{15}N-NH$_4^+$ was insignificant, the seasonal trend of the equilibrium fractionation coefficients between NH$_3$ and NH$_4^+$ was opposite to the seasonal trend of δ^{15}N-NH$_4^+$ of Qianliyan aerosols, and N was conserved during the non-oxidation reaction. Coal combustion contributed the most to the difference of Qianliyan aerosol nitrate δ^{15}N-NO$_3^-$ and ammonium δ^{15}N-NH$_4^+$ between summer and winter, which were due to the maximum change of its proportion in summer and winter and its ^{15}N isotope values.

The DIN deposition flux of Qianliyan aerosol was estimated to be 3.4 nmol N·m^{-2}·s^{-1}, which induced less than 1% to primary production. As aerosol inorganic nitrogen and N$_2$ fixation were considered as two sources of nitrate in the Yellow Sea thermocline in summer, aerosol inorganic nitrogen contributed some 80% of δ^{15}N-NO$_3^-$ depression of the summer Yellow Sea thermocline.

Data availability statement

The raw data supporting the conclusions of this article will be made available by the authors, without undue reservation.

Author contributions

KZ: assisting sample collections, laboratory analysis, data analysis, and running software. SL: funding, conceptualization,

and data analysis. NW: culturing denitrifying bacteria and data analysis. WX: running isotope ratio mass spectrometry and data analysis. All authors contributed to the article and approved the submitted version.

Conflict of interest

The authors declare that the research was conducted in the absence of any commercial or financial relationships that could be construed as a potential conflict of interest.

Publisher's note

All claims expressed in this article are solely those of the authors and do not necessarily represent those of their affiliated organizations, or those of the publisher, the editors and the reviewers. Any product that may be evaluated in this article, or claim that may be made by its manufacturer, is not guaranteed or endorsed by the publisher.

Supplementary material

The Supplementary Material for this article can be found online at: https://www.frontiersin.org/articles/10.3389/fmars.2022.993160/full#supplementary-material

References

Alexander, B., Sherwen, T., Holmes, C., Fisher, J., Chen, Q., Evans, M., et al. (2020). Global inorganic nitrate production mechanisms: Comparison of a global model with nitrate isotope observations. *Atmospheric Chem. Phys.* 20 (6), 3859–3877. doi: 10.5194/acp-20-3859-2020

Altieri, K. E., Fawcett, S. E., and Hastings, M. G. (2021). Reactive nitrogen cycling in the atmosphere and ocean. *Annu. Rev. Earth Planetary Sci.* 49, 523–550. doi: 10.1146/annurev-earth-083120-052147

Altieri, K. E., Hastings, M. G., Gobel, A. R., Peters, A. J., and Sigman, D. M. (2013). Isotopic composition of rainwater nitrate at Bermuda: The influence of air mass source and chemistry in the marine boundary layer. *J. Geophysical Res. Atmospheres* 118 (19), 11,304–11,316. doi: 10.1002/jgrd.50829

Altieri, K. E., Hastings, M. G., Peters, A. J., Oleynik, S., and Sigman, D. M. (2014). Isotopic evidence for a marine ammonium source in rainwater at Bermuda: Ammonium isotope in marine rain. *Global Biogeochem. Cycles* 28 (10), 1066–1080. doi: 10.1002/2014GB004809

Arteaga, L. A., Pahlow, M., Bushinsky, S. M., and Sarmiento, J. L. (2019). Nutrient controls on export production in the southern ocean. *Global Biogeochem. Cycles* 33 (8), 942–956. doi: 10.1029/2019GB006236

Asman, W. A. H., Sutton, M. A., and Schjørring, J. K. (1998). Ammonia: Emission, atmospheric transport and deposition. *New Phytol.* 139 (1), 27–48. doi: 10.1046/j.1469-8137.1998.00180.x

Aswini, A. R., and Hegde, P. (2021). Impact assessment of continental and marine air-mass on size-resolved aerosol chemical composition over coastal atmosphere: Significant organic contribution in coarse mode fraction. *Atmospheric Res.* 248, 105216. doi: 10.1016/j.atmosres.2020.105216

Bahm, K., and Khalil, M. A. K. (2004). A new model of tropospheric hydroxyl radical concentrations. *Chemosphere* 54 (2), 143–166. doi: 10.1016/j.chemosphere.2003.08.006

Bertram, T. H., Cochran, R. E., Grassian, V. H., and Stone, E. A. (2018). Sea spray aerosol chemical composition: Elemental and molecular mimics for laboratory studies of heterogeneous and multiphase reactions. *Chem. Soc. Rev.* 47 (7), 2374–2400. doi: 10.1039/c7cs00008a

Böhlke, J. K., Gwinn, C. J., and Coplen, T. B. (1993). New reference materials for nitrogen isotope ratio measurements. *Geostandards Newslett.* 17 (1), 159–164. doi: 10.1111/j.1751-908X.1993.tb00131.x

Böhlke, J. K., Mroczkowski, S. J., and Coplen, T. B. (2003). Oxygen isotopes in nitrate: new reference materials for $^{18}O:^{17}O:^{16}O$ measurements and observations on nitrate-water equilibration. *Rapid Commun. Mass Spectrometry* 17 (16), 1835–1846. doi: 10.1002/rcm.1123

Burger, J. M., Granger, J., Joyce, E., Hastings, M. G., Spence, K. A. M., and Altieri, K. E. (2022). The importance of alkyl nitrates and sea ice emissions to atmospheric NO_x sources and cycling in the summertime southern ocean marine boundary layer. *Atmospheric Chem. Phys.* 22 (2), 1081–1096. doi: 10.5194/acp-22-1081-2022

Carter, T. S., Joyce, E. E., and Hastings, M. G. (2021). Quantifying nitrate formation pathways in the equatorial pacific atmosphere from the GEOTRACES Peru-Tahiti transect. *ACS Earth Space Chem.* 5 (10), 2638–2651. doi: 10.1021/acsearthspacechem.1c00072

Casciotti, K. L., and McIlvin, M. R. (2007). Isotopic analyses of nitrate and nitrite from reference mixtures and application to Eastern Tropical North Pacific waters. *Mar. Chem.* 107 (2), 184–201. doi: 10.1016/j.marchem.2007.06.021

Chen, Y., Li, H., Karimian, H., Li, M., Fan, Q., Xu, Z., et al (2022). Spatio-temporal variation of ozone pollution risk and its influencing factors in China based on Geodetector and Geospatial models. *Chemosphere* 302, 134843. doi: 10.1016/j.chemosphere.2022.134843

Chang, C. P., Ha, K. J., Johnson, R. H., Kim, D., Lau, G. N. C., and Wang, B. (2021). The multiscale global monsoon system: World scientific series on Asia-pacific weather and climate. *World Sci.* 11, 12–36. doi: 10.1142/11723

Das, S. K., and Jayaraman, A. (2012). Long-range transportation of anthropogenic aerosols over eastern coastal region of India: Investigation of sources and impact on regional climate change. *Atmospheric Res.* 118, 68–83. doi: 10.1016/j.atmosres.2012.05.025

David Felix, J., Elliott, E. M., Gish, T. J., McConnell, L. L., and Shaw, S. L. (2013). Characterizing the isotopic composition of atmospheric ammonia emission sources using passive samplers and a combined oxidation-bacterial denitrifier approach: Improved method for isotope characterization of ammonia in air. *Rapid Commun. Mass Spectrometry* 27 (20), 2239–2246. doi: 10.1002/rcm.6679

Dobashi, T., Miyazaki, Y., Tachibana, E., Takahashi, K., Horii, S., Iwamoto, Y., et al. (2022). Marine nitrogen fixation as a possible source of atmospheric water-soluble organic nitrogen aerosols in the subtropical north pacific. EGUsphere [preprint]. doi: 10.21203/rs.3.rs-1342180/v2

Dong, X., Guo, Q., Han, X., Wei, R., and Tao, Z. (2022). The isotopic patterns and source apportionment of nitrate and ammonium in atmospheric aerosol. *Sci. Total Environ.* 803, 149559. doi: 10.1016/j.scitotenv.2021.149559

Duce, R. A., LaRoche, J., Altieri, K., Arrigo, K. R., Baker, A. R., Capone, D. G., et al. (2008). Impacts of atmospheric anthropogenic nitrogen on the open ocean. *Science* 320, 893–897. doi: 10.1126/science.1150369

Elliott, E. M., Kendall, C., Wankel, S. D., Burns, D. A., Boyer, E. W., Harlin, K., et al. (2007). Nitrogen isotopes as indicators of NO_x source contributions to atmospheric nitrate deposition across the Midwestern and northeastern united states. *Environ. Sci. Technol.* 41 (22), 7661–7667. doi: 10.1021/es070898t

Elliott, E. M., Yu, Z., Cole, A. S., and Coughlin, J. G. (2019). Isotopic advances in understanding reactive nitrogen deposition and atmospheric processing. *Sci. Total Environ.* 662, 393–403. doi: 10.1016/j.scitotenv.2018.12.177

Fan, M., Zhang, Y., Lin, Y., Cao, F., Zhao, Z., Sun, Y., et al. (2020). Changes of emission sources to nitrate aerosols in Beijing after the clean air actions: Evidence from dual isotope compositions. *J. Geophysical Research: Atmospheres* 125 (12), e2019JD031998. doi: 10.1029/2019JD031998

Felix, J. D., and Elliott, E. M. (2014). Isotopic composition of passively collected nitrogen dioxide emissions: Vehicle, soil and livestock source signatures. *Atmospheric Environ.* 92, 359–366. doi: 10.1016/j.atmosenv.2014.04.005

Freyer, H. D. (1991). Seasonal variation of $^{15}N/^{14}N$ ratios in atmospheric nitrate species. *Tellus B* 43 (1), 30–44. doi: 10.1034/j.1600-0889.1991.00003.x

Galloway, J. N. (2013). "The global nitrogen cycle," in *Treatise on geochemistry: Second edition*, (Jordan: Elsevier) vol. 10., 475–498. doi: 10.1016/B978-0-08-095975-7.00812-3

Galloway, J. N., Townsend, A. R., Erisman, J. W., Bekunda, M., Cai, Z., Freney, J. R., et al. (2008). Transformation of the nitrogen cycle: Recent trends, questions, and potential solutions. *Science* 320 (5878), 889–892. doi: 10.1126/science.1136674

Gobel, A. R., Altieri, K. E., Peters, A. J., Hastings, M. G., and Sigman, D. M. (2013). Insights into anthropogenic nitrogen deposition to the north Atlantic investigated using the isotopic composition of aerosol and rainwater nitrate: NITRATE ISOTOPES IN MARINE AEROSOLS. *Geophysical Res. Lett.* 40 (22), 5977–5982. doi: 10.1002/2013GL058167

Hastings, M. G., Sigman, D. M., and Lipschultz, F. (2003). Isotopic evidence for source changes of nitrate in rain at Bermuda: Nitrate N and O isotopes in Bermuda rain. *J. Geophysical Research: Atmospheres* 108 (D24), 4790. doi: 10.1029/2003JD003789

Heaton, T. H. E., Spiro, B., and Robertson, S. M. C. (1997). Potential canopy influences on the isotopic composition of nitrogen and sulphur in atmospheric deposition. *Oecologia* 109 (4), 600–607. doi: 10.1007/s004420050122

Jiang, D., Wang, H., and Lang, X. (2005). Evaluation of East Asian climatology as simulated by seven coupled models. *Adv. Atmospheric Sci.* 22 (4), 479–495. doi: 10.1007/BF02918482

Jickells, T. D., An, Z. S., Andersen, K. K., Baker, A. R., Bergametti, G., Brooks, N., et al. (2005). Global iron connections between desert dust, ocean biogeochemistry, and climate. *Science* 308 (5718), 67–71. doi: 10.1126/science.1105959

Joyce, E. E., Balint, S., and Hastings, M. G. (2022). Isotopic evidence that alkyl nitrates are important to aerosol nitrate formation in the Equatorial Pacific. *Geophysical Res. Lett.* 49, e2022GL099960. doi: 10.1029/2022GL099960

Kamezaki, K., Hattori, S., Iwamoto, Y., Ishino, S., Furutani, H., Miki, Y., et al. (2019). Tracing the sources and formation pathways of atmospheric particulate nitrate over the pacific ocean using stable isotopes. *Atmospheric Environ.* 209, 152–166. doi: 10.1016/j.atmosenv.2019.04.026

Karl, D., Letelier, R., Tupas, L., Dore, J., Christian, J., and Hebel, D. (1997). The role of nitrogen fixation in biogeochemical cycling in the subtropical north pacific ocean. *Nature* 388 (6642), 533–538. doi: 10.1038/41474

Kawashima, H. (2019). Seasonal trends of the stable nitrogen isotope ratio in particulate nitrogen compounds and their gaseous precursors in akita, Japan. *Tellus Ser. B: Chem. Phys. Meteorol.* 71 (1), 1–13. doi: 10.1080/16000889.2019.1627846

Kawashima, H., and Kurahashi, T. (2011). Inorganic ion and nitrogen isotopic compositions of atmospheric aerosols at yurihonjo, Japan: Implications for nitrogen sources. *Atmospheric Environ.* 45 (35), 6309–6316. doi: 10.1016/j.atmosenv.2011.08.057

Kawashima, H., and Ono, S. (2019). Nitrogen isotope fractionation from ammonia gas to ammonium in particulate ammonium chloride. *Environ. Sci. Technol.* 53 (18), 10629–10635. doi: 10.1021/acs.est.9b01569

Kim, H., Park, G. H., Lee, S. E., Kim, Y., Lee, K., Kim, Y. H., et al (2019). Stable isotope ratio of atmospheric and seawater nitrate in the East Sea in the Northwestern Pacific Ocean. *Mar. Pollut. Bull.* 149, 110610. doi: 10.1016/j.marpolbul.2019.110610

Knapp, A. N., Hastings, M. G., Sigman, D. M., Lipschultz, F., and Galloway, J. N. (2010). The flux and isotopic composition of reduced and total nitrogen in Bermuda rain. *Mar. Chem.* 120 (1-4), 83–89. doi: 10.1016/j.marchem.2008.08.007

Kundu, S., Kawamura, K., and Lee, M. (2010). Seasonal variation of the concentrations of nitrogenous species and their nitrogen isotopic ratios in aerosols at gosan, jeju island: Implications for atmospheric processing and source changes of aerosols. *J. Geophysical Res. Atmospheres* 115 (20), D20305. doi: 10.1029/2009JD013323

Lee, H. (2019). Isotopic characteristics of nitrate aerosols for tracing PM2.5 sources in South Korea (대한민국 PM2.5의 생성원 추적을 위한 질산염 에어로졸의 동위원소 특성 연구). [Master's thesis]. Seoul: Seoul National University (서울대학교). https://hdl.handle.net/10371/151599.

Lelieveld, J., Dentener, F. J., Peters, W., and Krol, M. C. (2004). On the role of hydroxyl radicals in the self-cleansing capacity of the troposphere. *Atmospheric Chem. Phys.* 4 (9/10), 2337–2344. doi: 10.5194/acp-4-2337-2004

Li, J., Davy, P., Harvey, M., Katzman, T., Mitchell, T., and Michalski, G. (2021). Nitrogen isotopes in nitrate aerosols collected in the remote marine boundary layer: Implications for nitrogen isotopic fractionations among atmospheric reactive nitrogen species. *Atmospheric Environ.* 245, 118028. doi: 10.1016/j.atmosenv.2020.118028

Li, Z., Walters, W. W., Hastings, M. G., Zhang, Y., Song, L., Liu, D., et al (2019). Nitrate isotopic composition in precipitation at a Chinese Megacity: Seasonal variations, atmospheric processes, and implications for sources. *Earth Space Sci.* 6 (11), 2200–13. doi: 10.1029/2019EA000759

Lin, C. T., Jickells, T. D., Baker, A. R., Marca, A., and Johnson, M. T. (2016). Aerosol isotopic ammonium signatures over the remote Atlantic ocean. *Atmospheric Environ.* 133, 165–169. doi: 10.1016/j.atmosenv.2016.03.020

Liu, S. M., Zhang, J., Chen, S. Z., Chen, H. T., Hong, G. H., Wei, H., et al. (2003). Inventory of nutrient compounds in the yellow Sea. *Continental Shelf Res.* 23 (11-13), 1161–1174. doi: 10.1016/S0278-4343(03)00089-X

Luo, H., Lao, Q., Chen, F., Chen, C., Zhou, X., Jin, G., et al. (2022). Nitrate sources and formation in aerosol and precipitation in a tropical city in south China: Insight from nitrate dual isotopes. *Atmospheric Environ.* 278, 119087. doi: 10.1016/j.atmosenv.2022.119087

Michalski, G., Bhattacharya, S. K., and Girsch, G. (2014). NO_x cycle and the tropospheric ozone isotope anomaly: An experimental investigation. *Atmospheric Chem. Phys.* 14 (10), 4935–4953. doi: 10.5194/acp-14-4935-2014

Michalski, G., Böhlke, J. K., and Thiemens, M. (2004). Long term atmospheric deposition as the source of nitrate and other salts in the atacama desert, Chile: New evidence from mass-independent oxygen isotopic compositions. *Geochimica Cosmochimica Acta* 68 (20), 4023–4038. doi: 10.1016/j.gca.2004.04.009

Mohamed, A. M. O., Maraqa, M. A., Howari, F. M., and Paleologos, E. K. (2021). "Outdoor air pollutants," in *Pollution assessment for sustainable practices in applied sciences and engineering*, (United Kingdom: Butterworth-Heinemann)491–554. doi: 10.1016/b978-0-12-809582-9.00009-8

Morin, S., Savarino, J., Frey, M. M., Domine, F., Jacobi, H. W., Kaleschke, L., et al. (2009). Comprehensive isotopic composition of atmospheric nitrate in the Atlantic ocean boundary layer from 65°S to 79°N. *J. Geophysical Res.* 114 (D5), D05303. doi: 10.1029/2008JD010696

O'Dowd, C. D. (2002). A dedicated study of new particle formation and fate in the coastal environment (PARFORCE): Overview of objectives and achievements. *J. Geophysical Res.* 107 (D19), 8108. doi: 10.1029/2001JD000555

Pan, Y., Gu, M., He, Y., Wu, D., Liu, C., Song, L., et al. (2020). Revisiting the concentration observations and source apportionment of atmospheric ammonia. *Adv. Atmospheric Sci.* 37 (9), 933–938. doi: 10.1007/s00376-020-2111-2

Pan, Y., Tian, S., Liu, D., Fang, Y., Zhu, X., Zhang, Q., et al. (2016). Fossil fuel combustion-related emissions dominate atmospheric ammonia sources during severe haze episodes: Evidence from ^{15}N-stable isotope in size-resolved aerosol ammonium. *Environ. Sci. Technol.* 50 (15), 8049–8056. doi: 10.1021/acs.est.6b00634

Park, Y., Park, K., Kim, H., Yu, S., Noh, S., Kim, M., et al. (2018). Characterizing isotopic compositions of TC-c, NO_3^--N, and NH_4^+-n in PM$_{2.5}$ in south Korea: Impact of china's winter heating. *Environ. pollut.* 233, 735–744. doi: 10.1016/j.envpol.2017.10.072

Parnell, A. C., Inger, R., Bearhop, S., and Jackson, A. L. (2010). Source partitioning using stable isotopes: Coping with too much variation. *PloS One* 5 (3), e9672. doi: 10.1371/journal.pone.0009672

Pöschl, U. (2005). Atmospheric aerosols: composition, transformation, climate and health effects. *Angew Chem. Int. Ed Engl.* 44 (46), 7520–7540. doi: 10.1002/anie.200501122

Qi, J., Yu, Y., Yao, X., and Gang, Y. (2020). Dry deposition fluxes of inorganic nitrogen and phosphorus in atmospheric aerosols over the marginal seas and Northwest pacific. *Atmospheric Res.* 245, 105076. doi: 10.1016/j.atmosres.2020.105076

Refulio-Coronado, S., Lacasse, K., Dalton, T., Humphries, A., Basu, S., Uchida, H., et al. (2021). Coastal and marine socio-ecological systems: A systematic review of the literature. *Front. Mar. Sci.* 8. doi: 10.3389/fmars.2021.648006

Savard, M. M., Cole, A., Smirnoff, A., and Vet, R. (2017). δ^{15}N values of atmospheric n species simultaneously collected using sector-based samplers distant from sources - isotopic inheritance and fractionation. *Atmospheric Environ.* 162, 11–22. doi: 10.1016/j.atmosenv.2017.05.010

Savarino, J., Morin, S., Erbland, J., Grannec, F., Patey, M. D., Vicars, W., et al. (2013). Isotopic composition of atmospheric nitrate in a tropical marine boundary layer. *Proc. Natl. Acad. Sci.* 110 (44), 17668–17673. doi: 10.1073/pnas.1216639110

Savoie, D. L., and Prospero, J. M. (1982). Particle size distribution of nitrate and sulfate in the marine atmosphere. *Geophysical Res. Lett.* 9 (10), 1207–1210. doi: 10.1029/GL009i010p01207

Schulz, H., Gehre, M., Hofmann, D., and Jung, K. (2001). Nitrogen isotope ratios in pine bark as an indicator of n emissions from anthropogenic sources. *Environ. Monit Assess.* 69, 283–297. doi: 10.1023/A:1010705907525

Seinfeld, J. H., and Pandis, S. N. (2016). *Atmospheric chemistry and physics: From air pollution to climate change* (Hoboken: John Wiley and Sons).

Seok, M. W., Kim, D., Park, G. H., Lee, K., Kim, T. H., Jung, J., et al. (2021). Atmospheric deposition of inorganic nutrients to the Western north pacific ocean. *Sci. Total Environ.* 793, 148401. doi: 10.1016/j.scitotenv.2021.148401

Sigman, D. M., Casciotti, K. L., Andreani, M., Barford, C., Galanter, M., and Böhlke, J. K. (2001). A bacterial method for the nitrogen isotopic analysis of nitrate in seawater and freshwater. *Analytical Chem.* 73 (17), 4145–4153. doi: 10.1021/ac010088e

Ti, C., Gao, B., Luo, Y., Wang, X., Wang, S., and Yan, X. (2018). Isotopic characterization of NH_x-n in deposition and major emission sources. *Biogeochemistry* 138 (1), 85–102. doi: 10.1007/s10533-018-0432-3

Walters, W. W., Chai, J., and Hastings, M. G. (2019). Theoretical phase resolved ammonia-ammonium nitrogen equilibrium isotope exchange fractionations: Applications for tracking atmospheric ammonia gas-to-particle conversion. *ACS Earth Space Chem.* 3 (1), 79–89. doi: 10.1021/acsearthspacechem.8b00140

Walters, W. W., Fang, H., and Michalski, G. (2018). Summertime diurnal variations in the isotopic composition of atmospheric nitrogen dioxide at a small midwestern united states city. *Atmospheric Environ.* 179, 1–11. doi: 10.1016/j.atmosenv.2018.01.047

Walters, W. W., and Michalski, G. (2015). Theoretical calculation of nitrogen isotope equilibrium exchange fractionation factors for various NO_y molecules. *Geochimica Cosmochimica Acta* 164, 284–297. doi: 10.1016/j.gca.2015.05.029

Walters, W. W., and Michalski, G. (2016). Theoretical calculation of oxygen equilibrium isotope fractionation factors involving various NO_y molecules, OH, and H_2O and its implications for isotope variations in atmospheric nitrate. *Geochimica Cosmochimica Acta* 191, 89–101. doi: 10.1016/j.gca.2016.06.039

Wang, Y., Liu, D., Xiao, W., Zhou, P., Tian, C., Zhang, C., et al. (2021). Coastal eutrophication in China: Trend, sources, and ecological effects. *Harmful Algae* 107, 102058. doi: 10.1016/j.hal.2021.102058

Wu, S. P., Zhu, H., Liu, Z., Dai, L. H., Zhang, N., Schwab, J. J., et al. (2019b). Nitrogen isotope composition of ammonium in $PM_{2.5}$ in the Xiamen, China: Impact of non-agricultural ammonia. *Environ. Sci. pollut. Res.* 26 (25), 25596–25608. doi: 10.1007/s11356-019-05813-8

Wu, Z., Yu, Z., Song, X., Wang, W., Zhou, P., Cao, X., et al. (2019a). Key nitrogen biogeochemical processes in the south yellow Sea revealed by dual stable isotopes of nitrate. *Estuarine Coast. Shelf Sci.* 225, 106222. doi: 10.1016/j.ecss.2019.05.004

Xiao, H. W., Xie, L. H., Long, A. M., Ye, F., Pan, Y. P., Li, D. N., et al. (2015). Use of isotopic compositions of nitrate in TSP to identify sources and chemistry in south China Sea. *Atmospheric Environ.* 109, 70–78. doi: 10.1016/j.atmosenv.2015.03.006

Xiao, H., Zhu, R., Pan, Y., Guo, W., Zheng, N., Liu, Y., et al. (2020). Differentiation between nitrate aerosol formation pathways in a southeast Chinese city by dual isotope and modeling studies. *J. Geophysical Research: Atmospheres* 125 (13), e2020JD032604. doi: 10.1029/2020JD032604

Xin, M., Wang, B., Xie, L., Sun, X., Wei, Q., Liang, S., et al. (2019). Long-term changes in nutrient regimes and their ecological effects in the bohai Sea, China. *Mar. Pollut. Bull.* 146, 562–573. doi: 10.1016/j.marpolbul.2019.07.011

Xu, L., and Penner, J. E. (2012). Global simulations of nitrate and ammonium aerosols and their radiative effects. *Atmospheric Chem. Phys.* 12 (20), 9479–9504. doi: 10.5194/acp-12-9479-2012

Yan, M., Dong, S., Zhong, X. S., Ning, X., and Xin, Y. (2019). A study on particulate nitrogen isotope distribution, isotope characteristics and controlling factors in the southern Yellow Sea in summer. *Haiyang Xuebao* 41 (12), 14–25. doi: 10.3969/j.issn.0253-4193.2019.12.002

Yang, J. Y. T., Hsu, S. C., Dai, M. H., Hsiao, S. S. Y., and Kao, S. J. (2014). Isotopic composition of water-soluble nitrate in bulk atmospheric deposition at dongsha island: Sources and implications of external n supply to the northern south China Sea. *Biogeosciences* 11 (7), 1833–1846. doi: 10.5194/bg-11-1833-2014

Yeatman, S. G., Spokes, L. J., Dennis, P. F., and Jickells, T. D. (2001). Comparisons of aerosol nitrogen isotopic composition at two polluted coastal sites. *Atmospheric Environ.* 35 (7), 1307–1320. doi: 10.1016/S1352-2310(00)00408-8

Yu, Z., and Li, Y. (2021). Marine volatile organic compounds and their impacts on marine aerosol-a review. *Sci. Total Environ.* 768, 145054. doi: 10.1016/j.scitotenv.2021.145054

Zhang, L., Altabet, M. A., Wu, T., and Hadas, O. (2007a). Sensitive measurement of NH_4^{+} $^{15}N/^{14}N$ ($\delta^{15}NH_4^{+}$) at natural abundance levels in fresh and salt-waters. *Analytical Chem.* 79 (14), 5297–5303. doi: 10.1021/ac070106d

Zhang, R., Chen, M., Cao, J., Ma, Q., Yang, J., and Qiu, Y. (2012). Nitrogen fixation in the East China Sea and southern yellow Sea during summer 2006. *Mar. Ecol. Prog. Ser.* 447, 77–86. doi: 10.3354/meps09509

Zhang, J., Zhang, G. S., Bi, Y. F., and Liu, S. M. (2011). Nitrogen species in rainwater and aerosols of the yellow and East China seas: effects of the East Asian monsoon and anthropogenic emissions and relevance for the NW pacific ocean: Nitrogen species in atmospheric samples. *Global Biogeochem. Cycles* 25 (3), 2010GB003896. doi: 10.1029/2010GB003896

Zhang, G. S., Zhang, J., and Liu, S. M. (2007b). Characterization of nutrients in the atmospheric wet and dry deposition observed at the two monitoring sites over yellow Sea and East China Sea. *J. Atmospheric Chem.* 57 (1), 41–57. doi: 10.1007/s10874-007-9060-3

Zhao, Z. Y., Cao, F., Fan, M. Y., Zhang, W. Q., Zhai, X. Y., Wang, Q., et al. (2020). Coal and biomass burning as major emissions of NO_X in northeast China: Implication from dual isotopes analysis of fine nitrate aerosols. *Atmospheric Environ.* 242, 117762. doi: 10.1016/j.atmosenv.2020.117762

Zheng, X. D., Liu, X. Y., Song, W., Sun, X. C., and Liu, C. Q. (2018). Nitrogen isotope variations of ammonium across rain events: Implications for different scavenging between ammonia and particulate ammonium. *Environ. pollut.* 239, 392–398. doi: 10.1016/j.envpol.2018.04.015

Zhu, Y., Zhou, S., Li, H., Luo, L., Wang, F., Bao, Y., et al. (2021). Formation pathways and sources of size-segregated nitrate aerosols in a megacity identified by dual isotopes. *Atmospheric Environ.* 264, 118708. doi: 10.1016/j.atmosenv.2021.118708

Zong, Z., Tian, C., Sun, Z., Tan, Y., Shi, Y., Liu, X., et al. (2022). Long-term evolution of particulate nitrate pollution in north China: Isotopic evidence from 10 offshore cruises in the bohai Sea from 2014 to 2019. *J. Geophysical Research: Atmospheres* 127 (11), e2022JD036567. doi: 10.1029/2022JD036567

Zong, Z., Wang, X., Tian, C., Chen, Y., Fang, Y., Zhang, F., et al. (2017). First assessment of NO_x sources at a regional background site in north China using isotopic analysis linked with modeling. *Environ. Sci. Technol.* 51 (11), 5923–5931. doi: 10.1021/acs.est.6b06316